

5.3 Kontrolle rauschinduzierter Oszillationen in raum-zeitlichen Systemen

5.3.1 Halbleiter-Übergitter

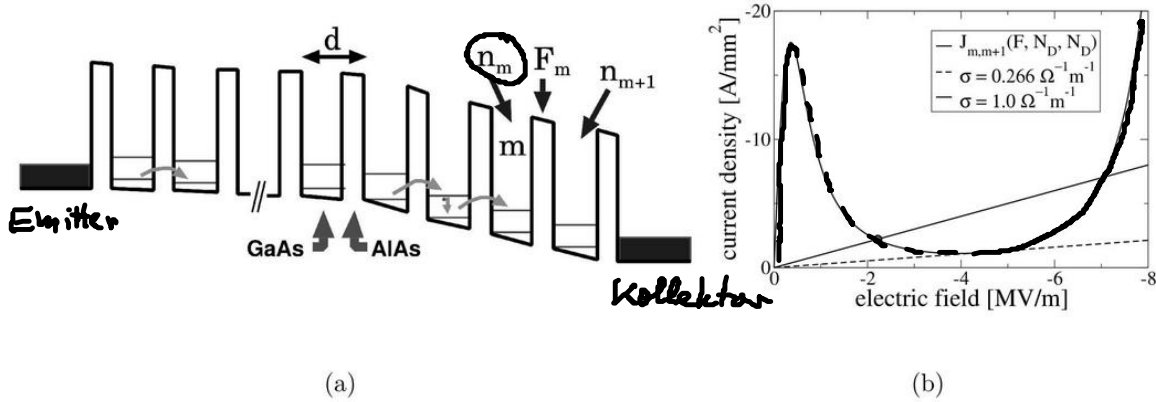


FIG. 1 (a) Superlattice energy band structure of alternating GaAs and AlAs layers under bias. (b) Current density vs electric field characteristic at the emitter barrier (straight line) and between two neutral wells exhibiting negative differential conductivity.

Hizanidis, Balanov, Amann, Schöll : PRL 96, 2444104 (2006)

$$\epsilon_0 \epsilon_s (F_m - F_{m-1}) = e (n_m - N_D)$$

$m = 1, \dots, N$

diskretes Gauß-Gesetz
 $e < 0$, Dotierungsdichte N_D [cm^{-2}]

$$e \dot{n}_m = J_{m-1 \rightarrow m} + D \xi_m(t) - J_{m \rightarrow m+1} - D \xi_{m+1}(t)$$

Ladungsträger-Kontinuitäts-gl. mit Gauß'schem weißen Rauschen $\langle \xi_m(t) \rangle = 0$

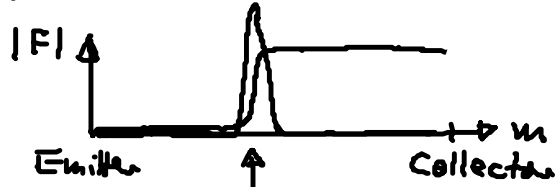
$$\langle \xi_m(t) \xi_{m'}(t') \rangle = \delta(t-t') \delta_{mm'}$$

resonante Tunnelstromdichte J

shot noise, thermal noise

Anwendung: Hochfrequenzoszillator

$D=0$: stationäre Felddomänen \rightarrow laufende Domänen



SNIPER-Bij.

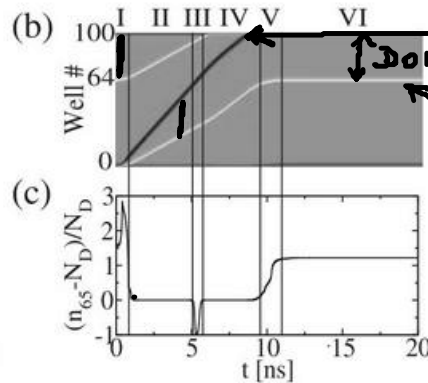
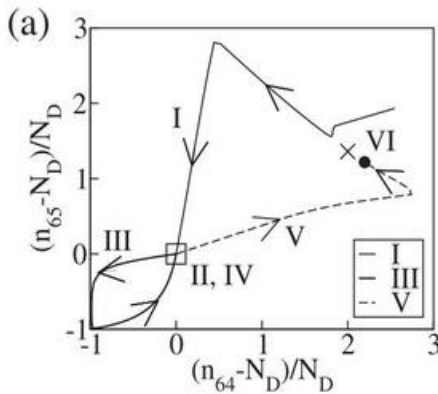
(wie gener. Modell in § 5.2)

Ladungsanreicherungsschicht (Front)
($n_m > N_D$)

globale Bedingung: Spannung

$$U_b = - \sum_{m=0}^N F_m d \quad F_m < 0$$

Ohm'sche Randbed. $J_{0 \rightarrow 1} = \sigma F_0$



Verarmungsfront
Domäne $n < N_D$
Anreicherungsfront
 $n > N_D$

FIG. 4. (a) Phase portrait in terms of electron densities n_{65} and n_{64} , normalized to the donor density N_D , below the global bifurcation. (b) Space-time plot and (c) time series of n_{65} for the trajectory shown in (a). The different parts of the trajectory are labeled by roman numerals I–VI in (a), (b), and (c). Parameters as in Fig. 1, $D = 0$.

$D \neq 0$: rauschinduzierte Domänen

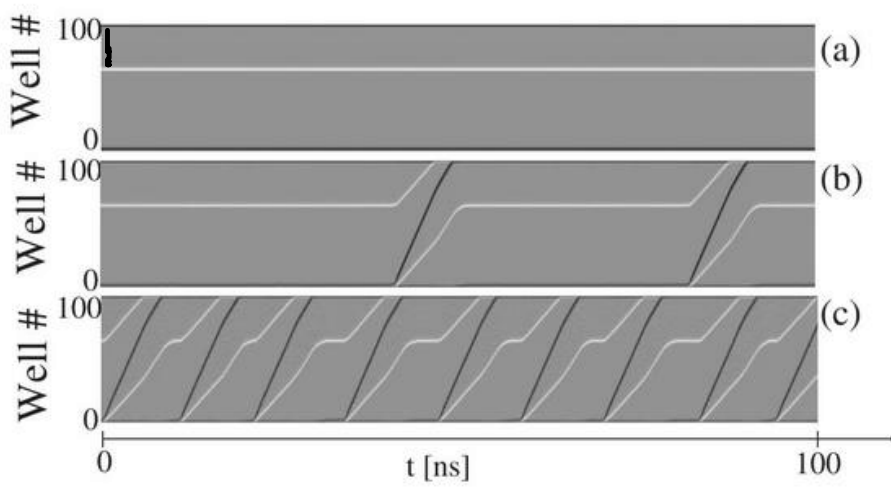


FIG. 1. Noise-induced front motion: Space-time plots of the electron density for (a) $D=0$ (no noise), (b) $D = 0.5 \text{ A s}^{1/2}/\text{m}^2$, and (c) $D = 2.0 \text{ A s}^{1/2}/\text{m}^2$. Light and dark shading corresponds to electron accumulation and depletion fronts, respectively. The emitter is at the bottom. Parameters: $U = 2.99 \text{ V}$, $\sigma = 2.0821012488 \text{ } \Omega^{-1} \text{ m}^{-1}$, $N_D = 10^{11} \text{ cm}^{-2}$, $T = 20 \text{ K}$, $N = 100$ GaAs wells of width $w = 8 \text{ nm}$, and $\text{Al}_{0.3}\text{Ga}_{0.7}\text{As}$ barriers of width $b = 5 \text{ nm}$, energies $E^a = 41.5 \text{ meV}$, $E^b = 160 \text{ meV}$, scattering width $\Gamma = 8 \text{ meV}$, transition matrix elements $H_{m,m+1}^{a,b} = -eF_m \times 0.0127 \text{ m}$, $H_{m+1,m}^{a,a} = -0.688 \text{ meV}$, $H_{m+1,m}^{b,b} = 1.263 \text{ meV}$, as in Ref. [9].

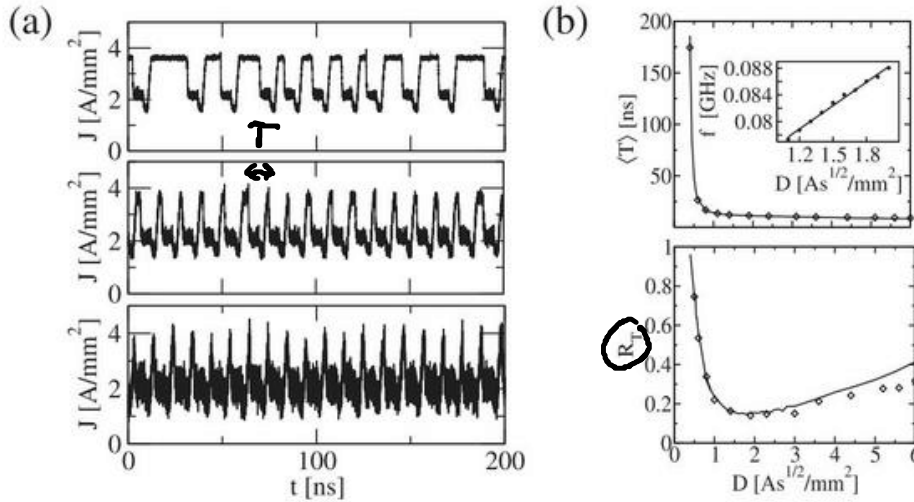
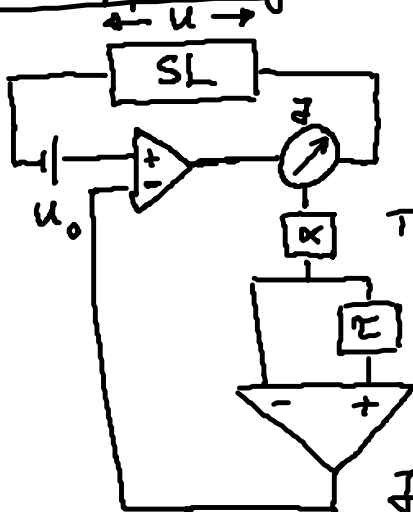


FIG. 2. (a) Three noise realizations of the current density $J(t)$. From top to bottom, $D = 0.8$, $D = 2.0$, and $D = 5.0 \text{ A s}^{1/2}/\text{m}^2$. (b) Mean interspike interval (top panel) and its normalized fluctuations R_T (bottom panel) versus noise intensity. Lines, constant D ; diamonds, $D \sim J_{m-1 \rightarrow m}^{1/2}$ [18]. The inset shows the peak frequency versus D .

Rückkopplungskontrolle



Tiefpassfilter $\bar{I} = \alpha \int_0^{t-t'} I(t') e^{-\alpha(t-t')} dt'$

(Abschneidefrequenz α)

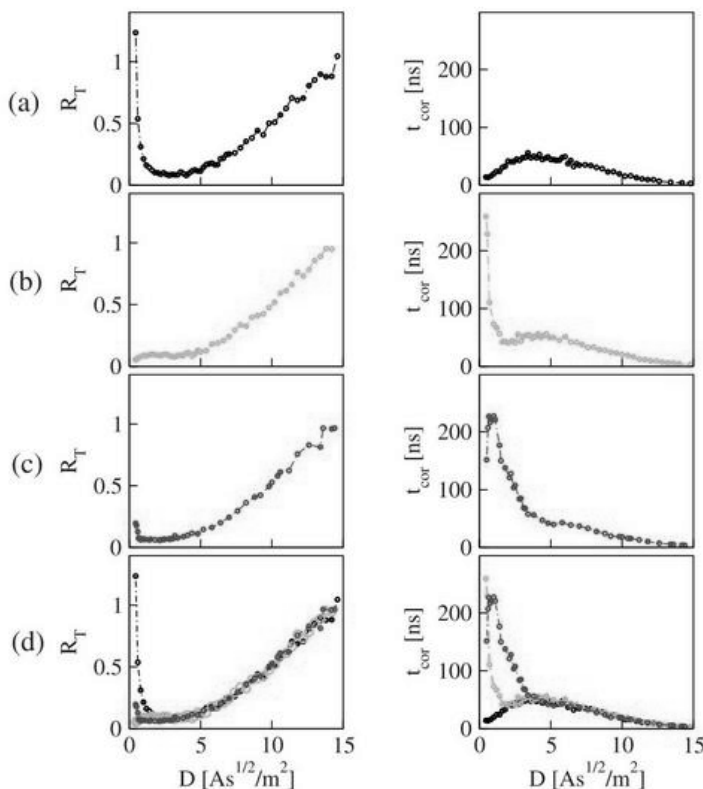
$$\bar{I} = \frac{1}{N+1} \sum_{m=0}^N \bar{I}_{m \rightarrow m+1}$$

Gesamtstrom (incl. Verschiebungsstrom)
 E. Schöll: Nonlin. Spatio-temp. Dyn. and Chaos
 in Semicond. (Cambridge 2007)

- Delay-induz. homokline Bif. zu laufenden Domänen
 (wie im gener. SNIPER-Modell)

- Kontrolle der Kohärenzresonanz

Hizanidis & Schöll, PRE 78, 066205 (2008)



$$K = 0$$

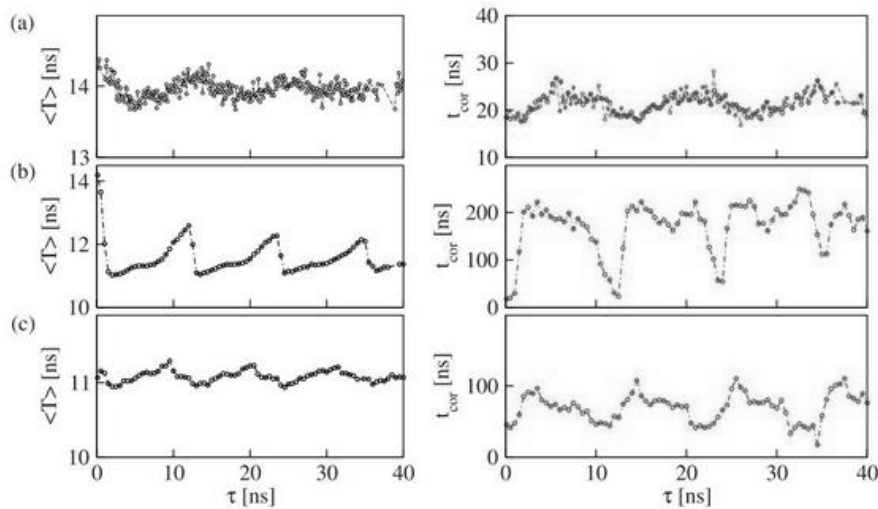
nichtoptimales τ
 \rightarrow Kohärenzresonanz
 zerstört

optimales τ
 \rightarrow Kohärenzresonanz
 verstärkt

(beide τ im
 delay-induz.
 Osc.-Regime)

FIG. 7. (Color online) Correlation time (right) and normalized fluctuation of pulse durations (left) as a function of the noise intensity for (a) $K=0$, (b) $(K, \tau)=(0.02 \text{ V mm}^2/\text{A}, 11 \text{ ns})$, and (c) $(K, \tau)=(0.02 \text{ V mm}^2/\text{A}, 14.5 \text{ ns})$. All three curves are plotted together in (d). Averages over 30 time series realizations of length

gether in (d). Averages over 30 time series realizations of length $T=1600$ ns have been used for the calculation of t_{cor} and averages over 1000 periods for R_T . $U=2.99$ V and $\sigma=2.0821$ ($\Omega \text{ m}$) $^{-1}$.



zu kleines K
 kleine Rauschint.
 große Rauschint.

FIG. 6. (Color online) Mean interspike interval $\langle T \rangle$ (left) and correlation time t_{cor} (right) in dependence on the time delay τ . (a) Control strength $K=0.002$ V mm 2 /A and noise intensity $D=1.0$ A s $^{1/2}$ /m 2 , (b) $K=0.02$ V mm 2 /A and $D=1.0$ A s $^{1/2}$ /m 2 , and (c) $K=0.02$ V mm 2 /A and $D=2.5$ A s $^{1/2}$ /m 2 . Averages over 30 time series realizations of length $T=1600$ ns have been used for the calculation of t_{cor} and averages over 1000 periods for $\langle T \rangle$. $U=2.99$ V and $\sigma=2.0821$ ($\Omega \text{ m}$) $^{-1}$.

5.3.2 Resonante Tunnelchode

Stegemann, Balenov, Schöll : PRE 71, 016221 (2005),
 PRE 73, 016203 (2006)
 Majer, Schöll : PRE 79, 011109 (2009)

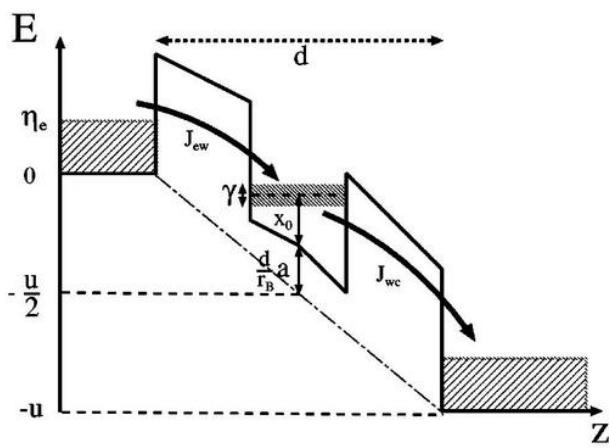
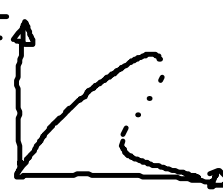


FIG. 1. Schematic energy band structure of the DBRT. The symbols are explained in the Appendix.

Double Barrier Resonant Tunneling Diode (DBRT)

Bandverbiegung durch Ladungsaussamml in QW

⇒ I-U-Char. z-förmige I-U-Char. (statt N-förmig)



Unkelbach et al, PRL 68, 026204 (2003)

$$\dot{a} = f(a, u) + D \frac{\partial^2 a}{\partial x^2} + D_a \zeta(x, t)$$

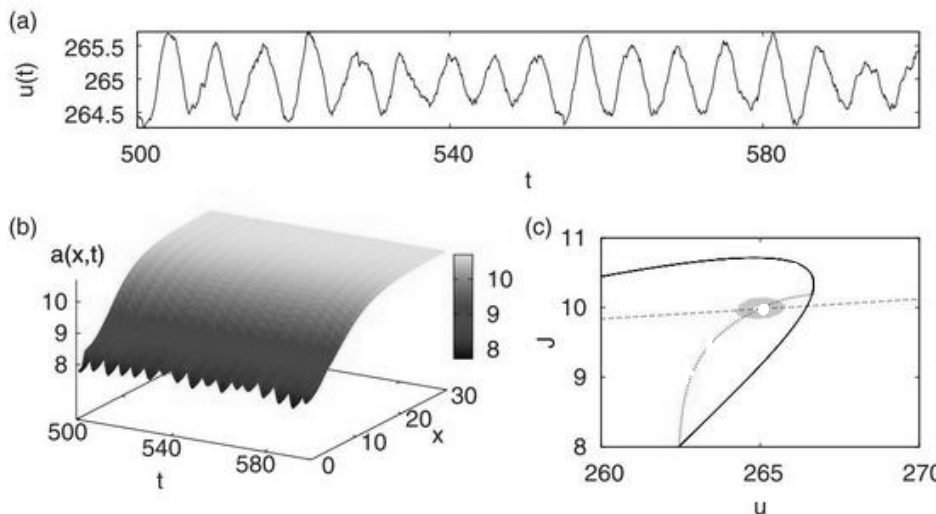
a Ladungsdichte

$$\dot{u} = \frac{1}{\epsilon} (u_0 - u - R J) + D_u \zeta(t) + K [u(t - \tau) - u(t)]$$

u Spannung
RC
 $\epsilon = \frac{\tau_a}{\tau_a}$
Kirchhoff
 $\tau_a = \text{Tunnelzeit}$
Rückkopplung über Strömung

Reaktions-Diff.-Modell mit globaler Kopplung $J = \frac{1}{L} \int_0^L j(a) dx$

- raum-zeitl. Dse. (breathing current filament) durch Hopf-Bif. ($D=K=0$)
- knapp unterhalb der Hopf-Bif. : rauschinduz. breathing ($K=0$)



Majer & Schöll
PRE (200)

FIG. 1. (Color online) Stochastic spatiotemporal dynamics under multiple time-delayed feedback control. (a) Voltage time series $u(t)$ (in units of 0.35 mV), (b) charge carrier density $a(x, t)$ (in units of 10^{10} cm^{-2}), (c) phase portrait of current I (in units of 500 A cm^{-2})

of 10^{-7} cm^{-2}), (c) phase portrait of current J (in units of 500 A/cm^2) vs voltage u . Space x and time t are scaled in units of 100 nm and 3.3 ps , respectively, corresponding to typical device parameters at 4 K [29]. Parameters are $U_0 = -84.2895$, $r = -35$, $\varepsilon = 6.2$, $D_u = 0.1$, $D_a = 10^{-4}$, $K = 0.1$, $\tau = 6.3$, $R = 0.5$.

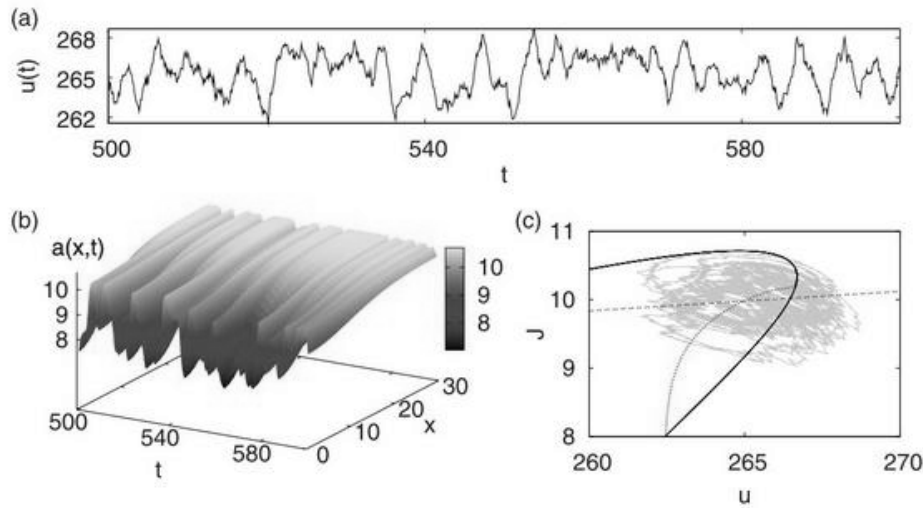


FIG. 2. (Color online) Same as Fig. 1 for $D_u = 1.0$.

• Vergrößerung von t_{cor} vs τ durch optimale τ

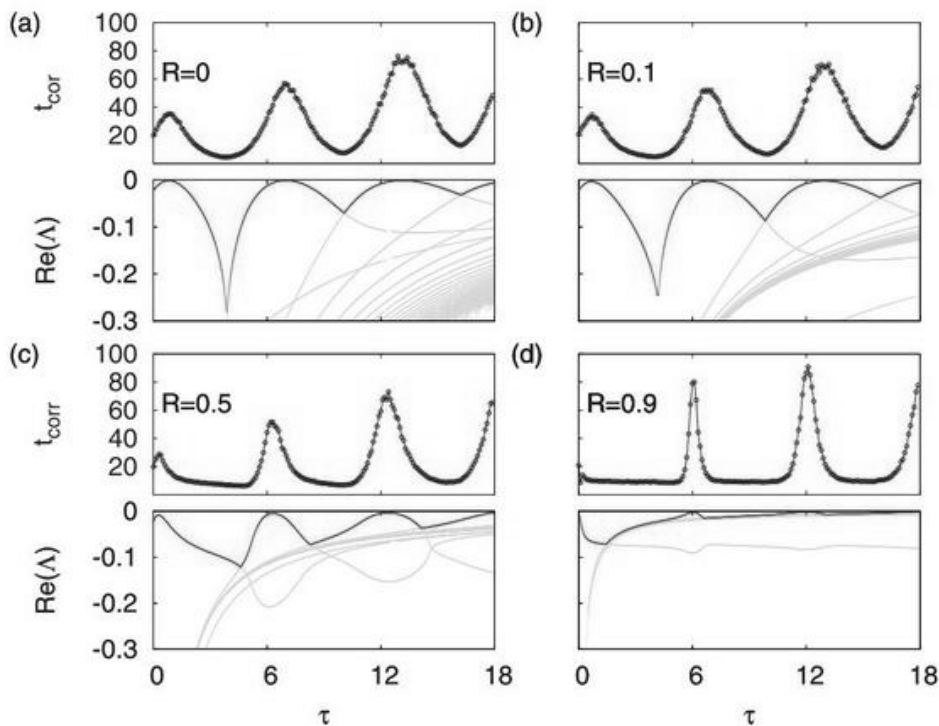


FIG. 7. (Color online) Correlation times t_{cor} (upper panels) and deterministic stability of the inhomogeneous fixed point, $\text{Re}(\Lambda)$ (lower panels), in dependence of the delay time τ for different values of the memory parameter R [(a)–(d)] and fixed $K = 0.1$. The red (dark) curves in the lower panels mark the leading eigenvalue, which governs the overall stability of the fixed point. Parameters: $\varepsilon = 6.2$, $D_u = 0.1$, and $D_a = 10^{-4}$ (in the panels showing t_{cor}).

$\varepsilon=6.2$, $D_u=0.1$, and $D_a=10^{-4}$ (in the panels showing t_{cor}).